



Transcription factor TAp73 and microRNA-449 complement each other to support multiciliogenesis

Merit Wildung¹ · Tilman Uli Esser¹ · Katie Baker Grausam^{2,3} · Cornelia Wiedwald¹ · Larisa Volceanov-Hahn¹ · Dietmar Riedel⁴ · Sabine Beuermann¹ · Li Li² · Jessica Zylla² · Ann-Kathrin Guenther⁵ · Magdalena Wienken⁶ · Evrim Ercetin¹ · Zhiyuan Han⁷ · Felix Bremmer⁸ · Orr Shomroni⁹ · Stefan Andreas¹ · Haotian Zhao^{2,3,7} · Muriel Lizé¹

Received: 23 April 2018 / Revised: 24 February 2019 / Accepted: 13 March 2019 / Published online: 8 May 2019
© ADMC Associazione Differenziamento e Morte Cellulare 2019

Abstract

Motile cilia serve vital functions in development, homeostasis, and regeneration. We recently demonstrated that TAp73 is an essential transcriptional regulator of respiratory multiciliogenesis. Here, we show that TAp73 is expressed in multiciliated cells (MCCs) of diverse tissues. Analysis of *TAp73* mutant animals revealed that TAp73 regulates *Foxj1*, *Rfx2*, *Rfx3*, axonemal dyneins *Dnali1* and *Dnai1*, plays a pivotal role in the generation of MCCs in male and female reproductive ducts, and contributes to fertility. However, the function of MCCs in the brain appears to be preserved despite the loss of *TAp73*, and robust activity of cilia-related networks is maintained in the absence of *TAp73*. Notably, *TAp73* loss leads to distinct changes in ciliogenic microRNAs: *miR34bc* expression is reduced, whereas the *miR449* cluster is induced in diverse multiciliated epithelia. Among different MCCs, choroid plexus (CP) epithelial cells in the brain display prominent *miR449* expression, whereas brain ventricles exhibit significant increase in *miR449* levels along with an increase in the activity of ciliogenic E2F4/MCIDAS circuit in *TAp73* mutant animals. Conversely, E2F4 induces robust transcriptional response from *miR449* genomic regions. To address whether increased *miR449* levels in the brain maintain the multiciliogenesis program in the absence of *TAp73*, we deleted both *TAp73* and *miR449* in mice. Although loss of *miR449* alone led to a mild ciliary defect in the CP, more pronounced ciliary defects and hydrocephalus were observed in the brain lacking both *TAp73* and *miR449*. In contrast, *miR449* loss in other MCCs failed to enhance ciliary defects associated with *TAp73* loss. Together, our study shows that, in addition to the airways, TAp73 is essential for generation of MCCs in male and female reproductive ducts, whereas *miR449* and TAp73 complement each other to support multiciliogenesis and CP development in the brain.

Introduction

Cilia are hair-like appendages protruding from the cell membrane into the surrounding environment. Solitary immotile primary cilia are a common organelle in most

mammalian cells, whereas motile cilia are restricted to a subset of cell types. This subset includes multiciliated cells (MCCs) lining brain ventricles, tracheal, and bronchial epithelium as well as the epithelium of male efferent ducts (EDs) and fallopian tubes (FTs) in females [1].

Multiciliogenesis requires precise regulation of the production, transport and assembly of a large number of different structural components, a process critically dependent on a hierarchical network of transcriptional and post-transcriptional regulators [2]. Geminin coiled-coil domain containing 1 (GEMC1) [3–5] and multiciliate differentiation and DNA synthesis associated cell cycle protein (MCIDAS or Multicilin) [6–8], members of the Geminin family, are early regulators of the MCC fate, downstream of the Notch pathway. MCC differentiation is also regulated by post-transcriptional mechanisms including microRNAs (miRNAs). *miR-34/449* constitutes a conserved family that encodes six homologous miRNAs

These authors contributed equally: Merit Wildung, Tilman Uli Esser

Edited by G. Melino

Supplementary information The online version of this article (<https://doi.org/10.1038/s41418-019-0332-7>) contains supplementary material, which is available to authorized users.

✉ Haotian Zhao
hzhao10@nyit.edu

✉ Muriel Lizé
mlize@gwdg.de

Extended author information available on the last page of the article.

(*miR34a*, *34b*, *34c*, *449a*, *449b*, and *449c*) from three genomic loci in vertebrates. Inhibition of the Notch pathway e.g., by *miR449* is required for multiciliogenesis through derepression of the transcriptional network of *GEMC1*, *MCIDAS*, E2F transcription factors (*E2F4*, *E2F5*), forkhead box J1 (*FOXJ1*), and v-myb avian myeloblastosis viral oncogene homolog (*MYB*) [9–11]. Disturbance of the molecular circuit leads to defective multiciliogenesis and ciliopathies in the airways, reproductive tracts, and the brain [1].

Transformation-related protein 73 (*Trp73*) is a member of the p53 family with distinct isoforms generated from two alternative promoters: isoforms containing the N-terminal transactivation domain (TAp73) and N-terminally truncated dominant-negative isoforms (Δ Np73). Recently, we and others showed that TAp73 is essential for airway multiciliogenesis [12, 13]. Gene expression analysis and chromatin immunoprecipitation (ChIP) identified TAp73 as a critical regulator of multiciliogenesis: TAp73 acts downstream of E2F4/MCIDAS and regulates the expression of *FOXJ1*, *RFX2*, and *RFX3* in pulmonary tissues [12, 14–17].

The FT of female reproductive tract consists of MCCs that possess hundreds of motile cilia beating in a wave-like manner which, along with musculature contraction, moves the oocyte or zygote towards the uterus [18–20]. Defects in ciliary functions may lead to ectopic pregnancies or infertility [19, 21]. In the male reproductive tract, MCCs in the EDs are involved in the transport of spermatozoa from testis to epididymis (Epi), their maturation and concentration [22–25].

MCCs in the brain can be found in a single layer of ependymal cells facing the ventricles and choroid plexus (CP). The CP epithelium, a specialized secretory epithelium that secretes cerebrospinal fluid, arises from monociliated progenitors in the roof plate around embryonic day (E) 12 and undergoes multiciliate differentiation to form multiple primary cilia [26, 27]. Ependymal cells in mice are specified around E16 and form multiple motile cilia on the apical surface after birth to facilitate cerebrospinal fluid movement [28, 29]. Defects in the ependymal and CP lineages are implicated in aging, hydrocephalus, and brain tumors [30, 31].

In this study, we detected robust TAp73 expression in MCCs in diverse tissues. In reproductive ducts, *TAp73* loss leads to a profound reduction of multiciliogenesis and suppression of *TAp73*-dependent transcriptional network activity. However, MCCs in the brain maintain robust multiciliogenesis activity despite *TAp73* loss. Molecular studies revealed alterations in *miR-34/449* family members in diverse MCCs from *TAp73* mutant mice: decreased levels of TAp73 target *miR34bc* concurrent with increased expression of *miR449*. In the brain, *miR449* is highly expressed in the CP and experiences significant upregulation following *TAp73* deletion. In addition, brain ventricles but no other multiciliated tissues from *TAp73* mutant animals exhibit increased expression of E2F4, which in turn is capable of eliciting

robust transcriptional response from *miR449* genomic loci, suggesting that *miR449* plays a crucial role in brain multiciliogenesis in collaboration with *TAp73*. Indeed, *miR449* loss alone results in ciliary reduction in the CP, whereas loss of both *TAp73* and *miR449* leads to a dramatic reduction of multiciliogenesis in the CP and severe hydrocephalus. Therefore, the molecular network governing MCC fate is subjected to tissue-specific feedback modulation by transcriptional and post-transcriptional mechanisms.

Materials and methods

Animals

TAp73 mutant mice with a targeted deletion of exons 2 and 3 of the *Trp73* gene were a generous gift from Dr. Tak Mak (Princess Margaret Cancer Centre, Toronto, Canada) [32]. *miR449* mutants were previously described [33]. Both strains were maintained in C57Bl/6 background (n8) at the animal facility of the European Neuroscience Institute Goettingen, Germany in full compliance with institutional guidelines. The study was approved by the Animal Care Committee of the University Medical Centre Goettingen and the authorities of Lower Saxony under the number 16/2069.

Human samples

Human Epi samples were procured with informed consent from two patients. All experimental procedures were approved and performed in accordance with the requirements set forth by the Ethics Committee of the University Medical Centre Goettingen (application number: 18/2/16).

Histology and immunostaining

Paraformaldehyde-fixed, paraffin-embedded tissues were treated with heat-induced epitope retrieval using Rodent Decloaker (RD913 L, Biocare Medical, Pacheco, CA, USA). For immunohistochemistry, endogenous peroxidase activity was quenched with 3% H₂O₂ for 10 min. Tissue sections were blocked with 10% fetal calf serum in phosphate-buffered saline with 0.1% Triton X-100, and subsequently incubated with primary antibodies (list of antibodies is provided in Supplementary Table 1). Biotinylated secondary antibodies were applied for 1 h at room temperature (list of antibodies is provided in Supplementary Table 2), after which avidin enzyme complex and substrate/chromogen were used for color development (Vector laboratories, Burlingame, CA, USA). Stained tissue sections were counterstained with hematoxylin. For immunofluorescence, sections were stained with fluorescently labeled secondary antibodies (list of antibodies is provided

in Supplementary Table 2) for 1 h at room temperature. Nuclei were counterstained with 4',6-diamidin-2-phenylindol (DAPI). Histology of tissue sections was assessed by using hematoxylin (Merck, Darmstadt, Germany) and eosin (Carl Roth, Karlsruhe, Germany) staining.

Electron microscopy

Transmission electron microscopy (TEM) was performed as previously described [12]. Briefly, murine tissue samples were fixed by immersion using 2% glutaraldehyde in 0.1 M cacodylate buffer (Science Services, München, Germany) at pH 7.4 overnight at 4 °C. Postfixation was performed using 1% osmium tetroxide diluted in 0.1 M cacodylate buffer. After pre-embedding staining with 1% uranyl acetate, tissue samples were dehydrated and embedded in Agar 100 (Plano, Wetzlar, Germany). Thin tissue sections (100 nm) were examined using a Philips CM 120 BioTwin transmission electron microscope (Philips Inc., Eindhoven, The Netherlands) and images were taken with a TemCam F416 CMOS camera (TVIPS, Gauting, Germany).

Quantification of cilia markers

Cilia were quantified using the *ImageJ* software [34]. Briefly, the region of interest was selected and a threshold was set to exclude unspecific background signals. The *Analyze Particles* tool was used to measure the area of the ciliary staining. Values were normalized to the length of the epithelia measured.

Western blot

Samples were homogenized in RIPA buffer (20 mM Tris-HCl pH 7.5, 150 mM NaCl, 9.5 mM EDTA, 1% Triton X-100, 0.1% SDS, 1% sodium deoxycholate) supplemented with urea (2.7 M) and protease inhibitors (Complete Mini EDTA-free, Roche, Basel, Switzerland). Equal amounts of protein extracts were separated by SDS-polyacrylamide gels prior to transfer onto a nitrocellulose membrane and incubated with primary antibodies (list of antibodies is provided in Supplementary Table 1). The membrane was washed and incubated for 1 h with horse radish peroxidase-conjugated secondary antibodies (list of antibodies is provided in Supplementary Table 2) followed by chemiluminescence detection. β -Actin or heat shock cognate 71 kDa protein (HSC70) was used as protein loading controls.

RNA extraction, quantitative PCR, small RNA sequencing, and RNAscope

Tissue samples were snap-frozen in liquid nitrogen and total RNA was isolated by Extrazol (7BioScience, Hartheim, Germany)/Chloroform extraction followed by 80% ethanol

precipitation at -20 °C. For cDNA synthesis, 1 μ g of total RNA was incubated with the M-MuLV reverse transcriptase and a mix of random nonameric and polyA tail primers at 42 °C for 1 h in a total volume of 50 μ l. All reactions were set up in triplicate with self-made SYBR Green quantitative PCR (qPCR) Mix (Tris-HCl [75 mM], $(\text{NH}_4)_2\text{SO}_4$ [20 mM], Tween-20 [0.01% v/v], MgCl_2 [3 mM], Triton X-100 [0.25% v/v], SYBR Green I (1:40 000), dNTPs [0.2 mM], and Taq polymerase [20 U/ml]) using 250 nM of each gene-specific primer (list of primers is provided in Supplementary Table 3). Standard curve method was used to assess relative transcript content. Transcript of interests was normalized to the reference transcript of ribosomal phosphoprotein P0 (Rplp0 or *36b4*) and normalized to the mean value of control samples. The results for each sample were obtained by averaging transcript levels of technical triplicates. No RT controls and dilution curves as well as melting curves and gel electrophoresis assessment of amplicons were performed for all primer combinations. For *miR449a*, *miR34b*, and *miR34c* quantification, the TaqMan miRNA Assay (Applied Biosystems, Thermo Fisher Scientific, Waltham, MA, USA) was performed according to the manufacturer's instructions with U6 snRNA as internal control.

Copy number in RNA samples was determined by qPCR using a murine TAp73 plasmid (MC219984, Origene, Rockville, USA) with a known copy number as standard curve. Copy number of the TAp73 plasmid was determined using the following formula: number of copies = (plasmid amount [ng] \times 6.022×10^{23} [molecules/mole]) / (plasmid length [bp] \times 1×10^9 [ng/g] \times 650 [g/mol])

The libraries for small RNA samples were prepared using the TruSeq Small RNA Library Prep Kit-Set A (24 rxns) (Set A: indexes 1–12; Cat N°: RS-200-001, Illumina, San Diego, CA, USA) using 1 μ g of total RNA according to the manufacturer's recommendations. Samples were sequenced on the Illumina HiSeq 4000 using a 50 bp single-end approach. Mapping, prediction of novel miRNAs, quality control, and differential expression (DE) analysis were carried out using Oasis2.0 (*Oasis: online analysis of small RNA deep sequencing data*) [35]. In brief, FASTQ files were trimmed with cutadapt 1.7.1 [36] removing TruSeq adapter sequences (TGGAATTCGGGTGCCAAGG) followed by removing sequences smaller than 15 or larger than 32 nucleotides. Trimmed FASTQ sequences were aligned to mouse small RNAs using STAR version 2.4.1d [37] with a mismatch of 5% of the sequence length and by utilizing the following databases: Mirbase version 21 for miRNAs; piRNAbank V.2 for piwiRNA; and Ensembl v84 for small nuclear RNA, small nucleolar RNA, and ribosomal RNA. Counts per small RNA were calculated using featureCounts v1.4.6 [38]. Novel miRNAs were searched using miRDeep2 version 2.0.0.5 [39]. DE of small RNA was determined by DESeq2 [40], where small RNAs were considered differentially expressed with an

adjusted p -value < 0.05 and absolute \log_2 fold change > 1 . The results of the DE analysis can be found in Supplementary Table S6, and the small RNA-seq data sets can be found in Gene Expression Omnibus with accession number **GSE108385**.

TAp73 (probe no. 475741), *Mcidas* (probe no. 510401-C2), *Hes1* (probe no. 417701), and *Hes5* (probe no. 400991-C2) were visualized using the RNAscope 2.5 HD Duplex Reagent Kit (#322430, Advanced Cell Diagnostics, Hayward, CA, USA) according to the manufacturer's instructions.

Chromatin immunoprecipitation (ChIP)

Chromatin was harvested from Saos2 cells transiently overexpressing TAp73 α , TAp73 β , and the control vector pcDNA3.1. Saos2 cells were routinely tested negative for Mycoplasma. ChIP and qPCR were performed as previously described using gene-specific primers (sequence information is provided in Supplementary Table 4) [12]. Enrichment levels were determined as the number of PCR products for each gene relative to total input.

Luciferase assay

The luciferase assay was performed as previously described [12]. Briefly, Saos2 cells were transfected with pcDNA3.1 empty vector, or pcDNA3.1 vector carrying *E2F4* or *MCIDAS*, or both *E2F4* and *MCIDAS* vectors. Moreover, a firefly luciferase reporter construct containing the putative three wild type E2F-binding sequences of *miR449* genomic region (wild type, or "WT"), or the same sequences lacking the strongest predicted E2F-binding motif (mutant, or "Mut") was transfected (sequence information is provided in Supplementary Table 5). In addition, a Renilla TK luciferase vector was co-transfected. At 24 h after transfection, cells were harvested and the luciferase activities were measured using the dual luciferase assay. Firefly luciferase activities were determined relative to those of Renilla TK luciferase vector and normalized to the mean value of samples from the control vector. Luciferase assays were performed as technical triplicates on every biological replicate.

Video microscopy

Murine FT and testis connected to the Epi were dissected and transferred to Dulbecco's Modified Eagle's Medium (DMEM, Gibco, Thermo Fisher Scientific, Waltham, MA, USA). To image spermatozoa, the Epi was separated from testis and vas deferens and an incision was made at distal end to release the spermatozoa. Spermatozoa as well as the peristaltic contraction of the FT were imaged with an inverse microscope.

Imaging of cilia-generated bead flow and cilia beating in the brain ventricular system

Mice brains were dissected and transferred to DMEM 21063 (Gibco, Thermo Fisher Scientific). Coronal slices containing the lateral ventricle, ventral third ventricle, aqueduct, and fourth ventricle were prepared by using a coronal adult brain matrix (ASI Instruments, Warren, MI, USA). The ventral third ventricle was processed further as previously described [41]. Tissue explant was placed in DMEM containing fluorescent latex beads (Fluoresbrite Multifluorescent 1.0 micron Microspheres, Polysciences, Warrington, PA, USA). Movement of fluorescent beads along the ventricular wall and within ventricular lumen was observed by fluorescence microscopy using a DMR (Leica, Wetzlar, Germany) upright microscope with an epifluorescence lamp. Ciliary beating was observed by differential interference contrast microscopy using the same set-up. Bead movement was recorded using a high-speed camera (Cascade II-512, Photometrics, Tucson, AZ, USA) operated by Multi-Recorder Software (developed by Johannes Schröder_Schetlig) and analyzed using ImageJ software [34].

Statistical analysis

One-tailed, unpaired Student's t -test assuming normal distribution, and equal variances were used to calculate statistical significance for pairwise comparisons. Luciferase assay statistics were assessed using one-way ANOVA assuming normal distribution followed by Dunnett's multiple comparison tests. The following indications of significance were used: * $P < 0.05$, ** $P < 0.01$, *** $P < 0.001$. N values represent biological replicates. Error bars indicate standard error of the mean (SEM).

Results

TAp73 is expressed in diverse multiciliated epithelia

We and others previously showed that TAp73 expressed in respiratory epithelia controls multiciliogenesis [12, 13]. However, little is known about the expression and function of TAp73 in other MCCs. To address this, we performed immunostaining and in situ hybridization and demonstrated that in addition to the testis [42, 43], TAp73 is expressed in EDs, FTs, and ependymal and CP epithelial cells in the brain (Fig. 1a–f; Supplementary Fig. 1). qPCR and western blot analyses showed that, among different multiciliated epithelia, FTs and EDs exhibit higher levels of TAp73 expression than testis or brain (Fig. 1g–i). Taken together, these results demonstrate robust TAp73 expression in different MCC types.

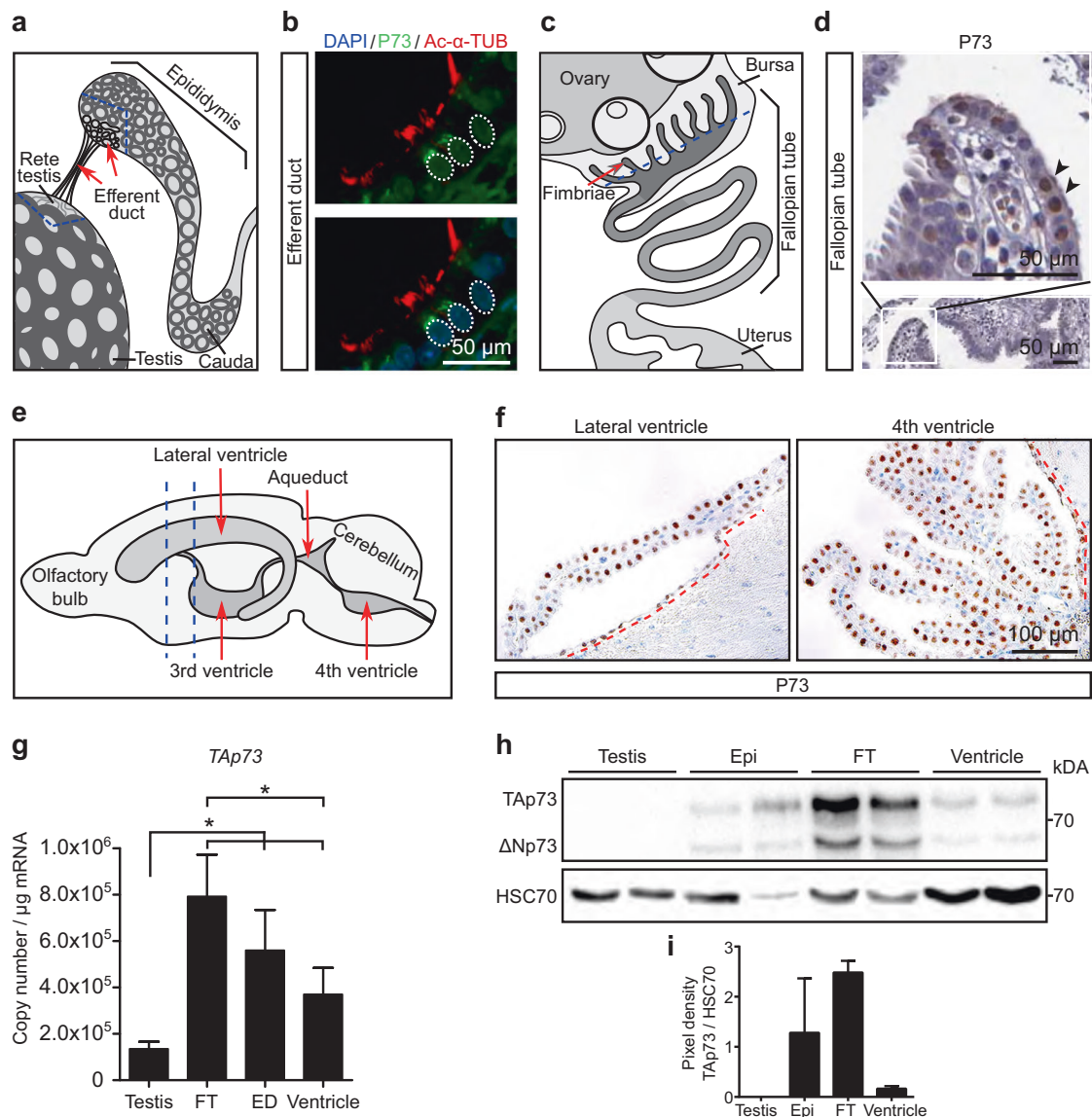


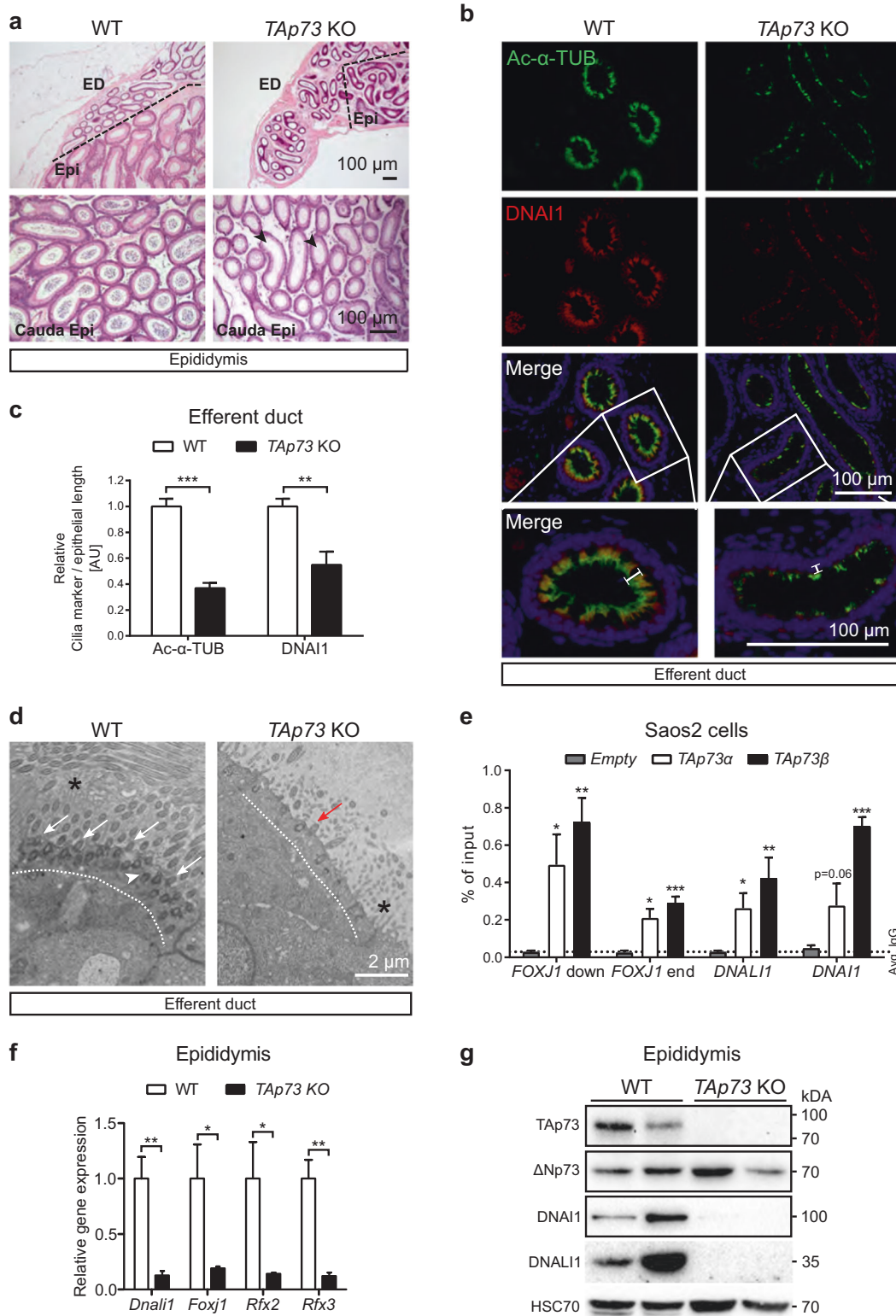
Fig. 1 TAp73 is expressed in diverse multiciliated epithelia. **a** Schematic illustration of efferent ducts (EDs, red arrows) that connect testis and epididymis (Epi). Blue dotted lines indicate regions used for histological, protein, and RNA analyses. **b** Representative images of the expression of P73 (green) and the axonemal marker acetylated alpha-tubulin (Ac- α -TUB, red) in the human ED. White bracket circles delineate P73 nuclear staining. DAPI staining (blue) marks nuclei. **c** Schematic illustration of the fallopian tube (FT) that connects ovary and uterus. Blue dotted line illustrates the region used for immunofluorescence analysis including fimbriae (red arrow). **d** Expression of P73 in human FT. Upper panel depicts a magnification of the boxed region in the lower panel. Arrowheads mark P73⁺ cells. Images were retrieved from Human Protein Atlas (<https://www.proteinatlas.org/ENSG00000078900-TP73/tissue/fallopian+tube>). **e** Schematic illustration of murine brain

ventricles (red arrows). Blue dotted lines indicate the position of coronal brain slices used in protein and RNA analyses. **f** Expression of TAp73 in lateral and fourth ventricles of wild type (WT) adult mice. Red dotted lines demarcate ependymal cells lining brain ventricles. Notice that both ependymal and choroid plexus (CP) epithelial cells express TAp73. **g** Quantitative PCR analysis of *TAp73* expression in the testis, EDs, FTs, and brain ventricles from WT adult mice. Expression levels are shown in copy number. Data from a single experiment are shown (testis, $n = 3$; FT and ventricle, $n = 4$; ED, $n = 6$). **h** Western blot analysis of the expression of TAp73 and ΔNp73 in testis, Epi, FT, and brain ventricle from WT adult mice. Heat shock cognate 71 kDa protein (HSC70) serves as a loading control. Data are representative of two independent experiments. **i** Quantitation of the signal intensity of TAp73 bands relative to that of HSC70 (**h**) is shown. All data are presented as mean \pm SEM with $*P < 0.05$

TAp73 is crucial for the molecular circuit of multiciliogenesis in efferent ducts

Loss of *TAp73* leads to male infertility that has been attributed to defective germ cell maintenance during

spermatogenesis [42, 43]. Interestingly, we detected spermatozoa in testis from *TAp73* knockout (KO) mice, although at a markedly reduced level (Supplementary Fig. 2a, b). Despite normal morphology and mobility of these cells, no mature spermatozoa were detected in the Epi



of these mice (Fig. 2a; Supplementary Video 1a–d), suggesting that additional defects may contribute to infertility. The multiciliated epithelium of the EDs contributes to

gamete transport by facilitating testicular fluid circulation, fluid reabsorption, and spermatozoa concentration [22, 24, 25], all essential aspects of male fertility

◀ **Fig. 2** TAp73 controls multiciliogenesis in the male reproductive tract. **a** Representative images of hematoxylin and eosin (H&E) staining of Epi sections from WT and *TAp73* knockout (KO) animals. Bracket lines demarcate the border of EDs and Epi. Notice the lack of mature spermatozoa in cauda Epi from *TAp73* KO mice (arrowheads). **b** Representative images of the expression of Ac- α -TUB (green) and axonemal dynein DNAI1 (red) in EDs from WT and *TAp73* KO mice. DAPI staining (blue) labels nuclei. Boxed regions are magnified in the bottom panel. Note that *TAp73* KO mice have less cilia that also exhibit reduced length (white bars). **c** Quantitation of Ac- α -TUB and DNAI1 signals normalized to epithelial length. Data from a single experiment are shown (WT, $n = 6$ images from 3 animals; *TAp73* KO, $n = 11$ images from 4 animals). **d** Representative photomicrographs of transmission electron microscopy (TEM) in EDs from WT and *TAp73* KO mice. Dotted lines mark apical region of the cells. Notice the abundant cilia (white arrows) and clustered basal bodies (white arrowhead) docked to the apical surface of WT cells, whereas mutant cells exhibit fewer cilia (red arrow). Interspersed microvilli are marked with asterisks. **e** Chromatin immunoprecipitation was performed for Saos2 cells transfected with TAp73 α , TAp73 β , and empty vector. Binding of TAp73 α and TAp73 β to genomic regions of *FOXJ1*, axonemal dyneins *DNALI1* and *DNAI1* was evaluated by quantitative PCR and compared to vector control ($n = 3$ for each antibody/gene pair, except for *DNALI1* [$n = 4$], genomic regions examined are illustrated in Supplementary Fig. 3; [78]). **f** Semiquantitative PCR analysis of *Dnali1*, *Foxj1*, *Rfx2*, and *Rfx3* expression in EDs from WT and *TAp73* KO mice. Data from a single experiment are shown (WT, $n = 4$ for *Dnali1*, *Foxj1*, and *Rfx3*, $n = 3$ for *Rfx2*; *TAp73* KO, $n = 3$). **g** Immunoblot analysis of the expression of TAp73, Δ Np73, DNAI1, and DNALI1 in Epi from WT and *TAp73* KO animals. HSC70 serves as a loading control. Representative result of three independent experiments is displayed. All data are presented as mean \pm SEM and relative to the WT group with * $P < 0.05$, ** $P < 0.01$, *** $P < 0.001$

[9, 44, 45]. Indeed, though no gross morphological difference was observed in EDs between control and *TAp73* KO animals (Fig. 2a), immunofluorescent staining of the cilia components acetylated alpha-tubulin (Ac- α -TUB) and dynein axonemal intermediate chain 1 (DNAI1) showed a dramatic reduction in the number and length of cilia in the EDs from *TAp73* KO mice (Fig. 2b, c). In contrast to the abundant long cilia of WT cells, mutant MCCs generated far fewer cilia as observed by TEM (Fig. 2d; Supplementary Fig. 2c), resembling the loss of airway cilia in these animals [12]. Consistent with its role as transcriptional regulator, ChIP followed by qPCR revealed significant enrichment of TAp73 in genomic loci of *FOXJ1* [12] and dynein axonemal light intermediate chain 1 (*DNALI1*) and *DNAI1*, both encoding axonemal dyneins (Fig. 2e; Supplementary Fig. 3). Accordingly, expression of *Dnali1*, *Foxj1*, *Rfx2*, and *Rfx3* was reduced or almost completely lost in male reproductive ducts from *TAp73* KO animals (Fig. 2f, g; Supplementary Fig. 2d). Together, our data indicate that TAp73 directs *Dnali1* and *Dnai1* in addition to known critical nodes including *Foxj1*, *Rfx2*, and *Rfx3* to mediate multiciliogenesis in EDs (Fig. 7a, b). Thus, these additional defects in the multiciliated epithelium of the EDs may contribute to male infertility in *TAp73* KO mice.

TAp73-driven transcriptional network regulates multiciliogenesis in fallopian tubes

Though infertility in *TAp73* KO females is thought to arise from defects of oocyte development and release from the ovary [32, 46], it remains unclear whether *TAp73* loss affects the multiciliated epithelium of the FT, thereby possibly influencing ova transport. Despite normal tubal morphology, analysis of Ac- α -TUB and DNAI1 expression showed reduced cilia coverage of the oviduct epithelium (Fig. 3a–c). Consistently, TEM demonstrated reduced cilia and mislocated basal bodies in FTs from *TAp73* KO mice (Fig. 3d; Supplementary Fig. 4a). Transcript levels of *Dnali1*, *Foxj1*, and *Rfx2*, but not *Rfx3*, were reduced in *TAp73* KO FTs (Fig. 3e), which were accompanied by declined protein expression of FOXJ1, DNAI1, DNALI1 (all expressed in the human FTs, Supplementary Fig. 4b), and gamma-tubulin (γ -TUB, basal body marker) (Fig. 3f), though to a lesser degree when compared to the decrease in multiciliogenesis activity observed in *TAp73*-deficient EDs. Further, smooth muscle contraction pattern in FTs is similar between control and *TAp73* KO animals (Supplementary Video 2a, b). Taken together, our data indicate that *TAp73* loss leads to reduced multiciliogenesis in the oviducts (Fig. 7a, c).

Ciliary function in the brain is intact in the absence of TAp73

Given TAp73 expression in ependymal and CP epithelial cells, we further evaluated TAp73 expression during embryonic brain development. Immunofluorescent studies showed that proliferative progenitors (KI-67⁺) are present in hindbrain roof plate at E14.5, whereas post-mitotic cells expressing aquaporin 1 (AQP1) [31, 47] are detected in CP epithelium (KI-67⁻/AQP1⁺) (Fig. 4a). Notably, a portion of the roof plate exists between the progenitors and CP epithelium that remains undifferentiated after cell cycle exit (KI-67⁻/AQP1⁻) (Fig. 4a). In contrast to progenitors with a solitary primary cilium, the “transition” zone is comprised of MCCs that exhibit TAp73 expression (Fig. 4b).

The expression of TAp73 in ependymal and CP epithelial cells, along with recent studies demonstrating the role of E2F4/MCIDAS in multiciliogenesis of ependymal cells [7, 48, 49], led us to examine the role of TAp73 in MCCs in the brain. Immunostainings confirmed the loss of TAp73 expression in ependymal cells and the CP from *TAp73* KO mice (Fig. 4c), whereas morphological analysis revealed no apparent defect in these cells (Supplementary Fig. 5a). We performed immunostainings for the cilia markers ADP-ribosylation factor-like 13b (ARL13B) [50], Ac- α -TUB, and DNAI1 in the fourth and lateral ventricles. In contrast to FTs and EDs, MCCs in ependyma and CP from *TAp73* KO

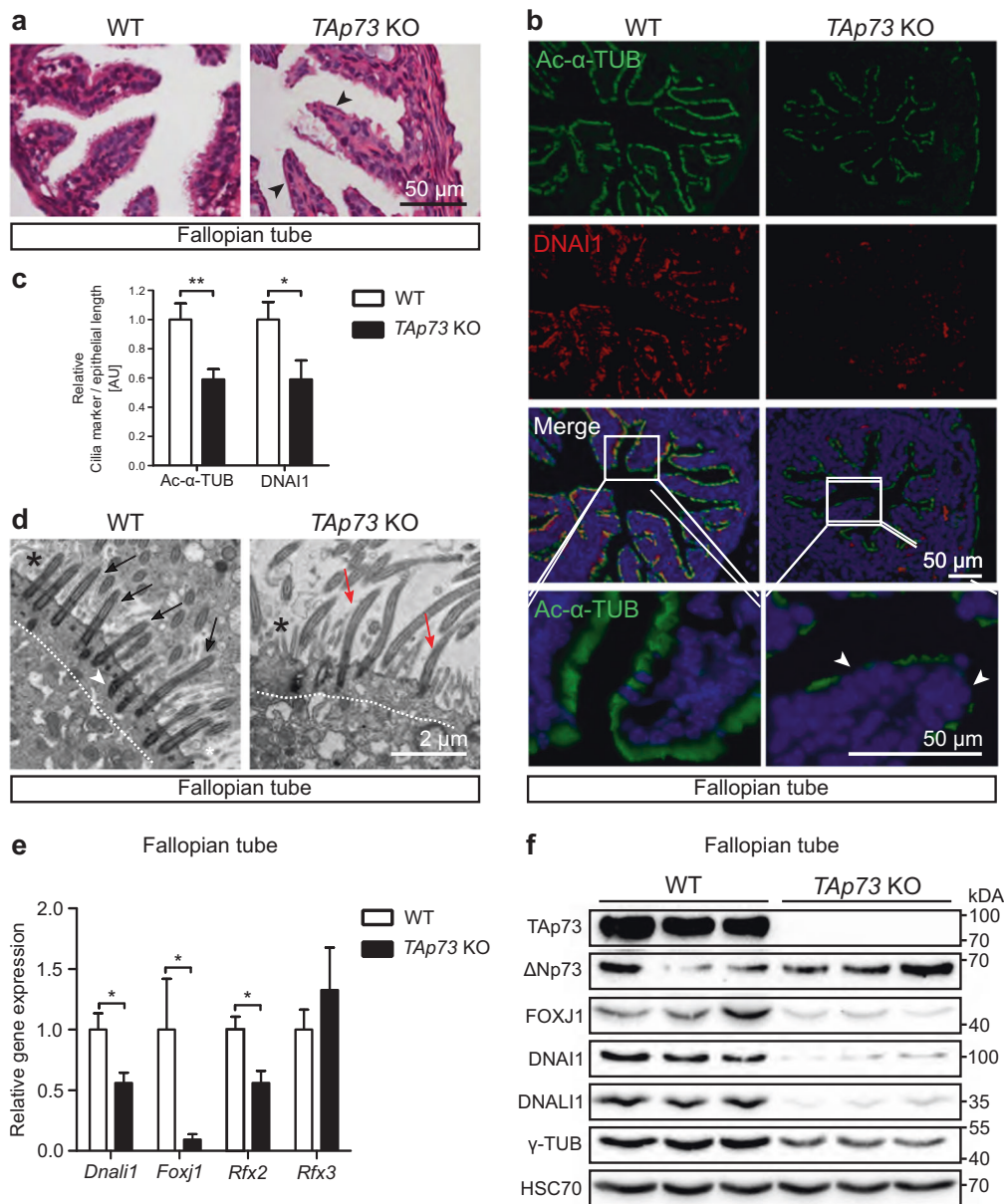
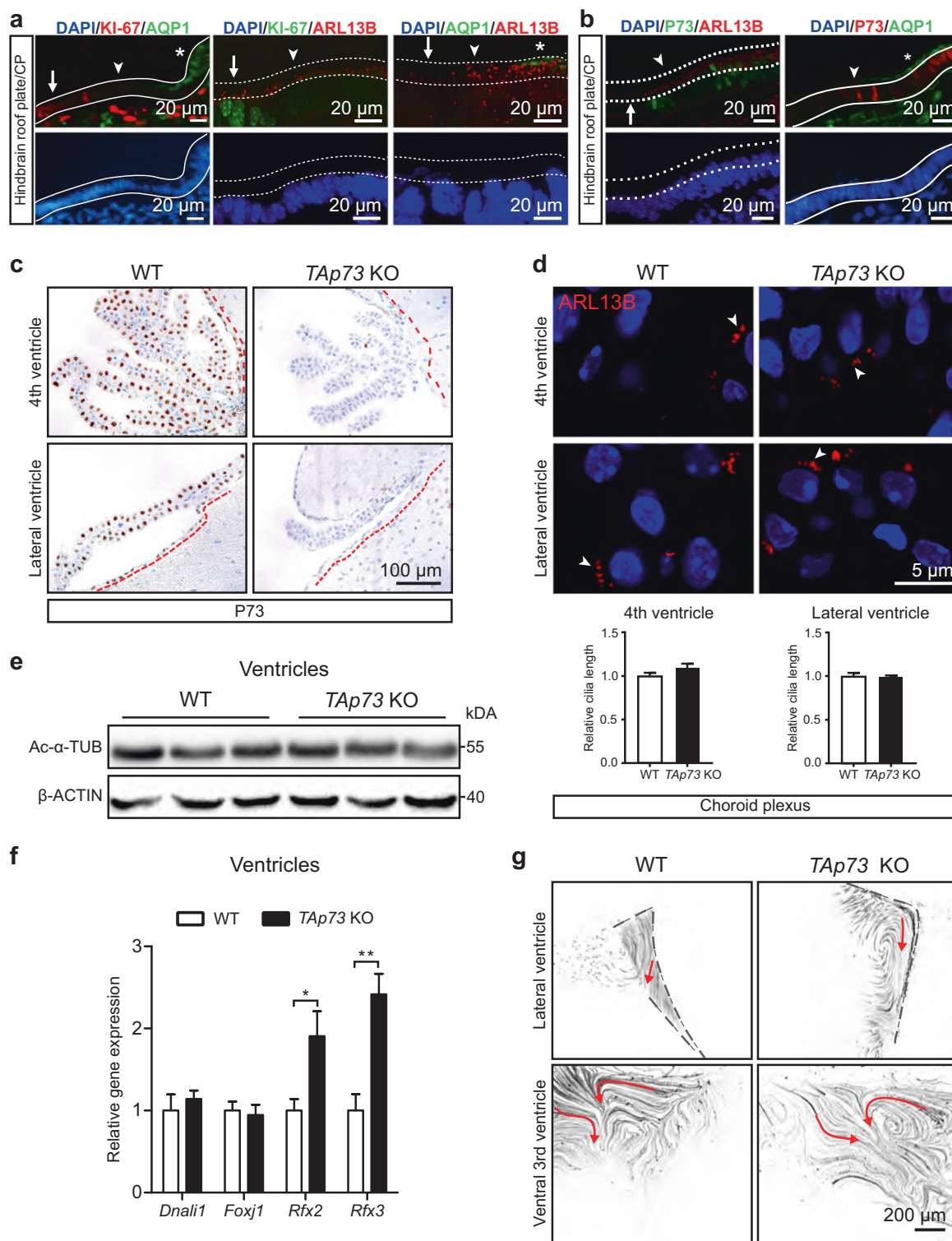


Fig. 3 TAp73 controls multiciliogenesis in the oviducts. **a** Representative H&E staining of FTs from WT and *TAp73* KO animals. **b** The expression of Ac- α -TUB (green) and DNAI1 (red) in FTs from WT and *TAp73* KO mice. DAPI staining (blue) labels nuclei. Boxed regions are magnified in the bottom panel. In contrast to multiciliated epithelia in WT mice, *TAp73* KO mice exhibit FT segments devoid of cilia (arrowheads). **c** Quantitation of Ac- α -TUB and DNAI1 signals normalized to epithelial length. Data from a single experiment are shown (WT, $n = 6$ images from 4 mice; *TAp73* KO, $n = 6$ images from 3 mice). **d** Representative TEM photomicrographs of FTs from WT and *TAp73* KO animals. Dotted lines mark apical region of the cells. Notice the presence of abundant cilia (black arrows) and basal bodies

(white arrowhead) docked at the apical surface of WT cells, whereas mutant cells display fewer cilia (red arrows). Interspersed microvilli are marked with asterisks. **e** Semiquantitative PCR analysis of *Dnali1*, *Foxj1*, *Rfx2*, and *Rfx3* expression in oviducts from WT and *TAp73* KO mice. Data from a single experiment are shown ($n = 3$). **f** Immunoblot analysis of the expression of TAp73, Δ Np73, FOXJ1, DNAI1, DNALI1, and gamma-tubulin (γ -TUB) in oviducts from WT and *TAp73* KO animals. HSC70 serves as a loading control. Data are representative of three independent experiments. All data are presented as mean \pm SEM and relative to the WT group with * $P < 0.05$, ** $P < 0.01$

animals are similar to those of WT mice (Fig. 4d, e; Supplementary Fig. 5b–d). No significant difference was observed in the expression of markers for epithelial differentiation of CP between control and *TAp73* KO animals

(Supplementary Fig. 6a–d). RT-qPCR analysis demonstrated similar expression levels of *Dnali1* and *Foxj1*, whereas increased *Rfx2* and *Rfx3* mRNA levels were observed in brain ventricles from *TAp73* KO mice (Fig. 4f). Consistently, ciliary



beating and bead flow in the cerebrospinal fluid appeared unaffected by *TAp73* loss (Fig. 4g; Supplementary Video 3a, b). Taken together, these results indicate that, unlike EDs, FTs, and the airways [12], the differentiation and function of MCCs in the brain remain intact despite *TAp73* loss.

***TAp73* regulates *miR-34/449* family members in diverse MCCs**

Functional MCCs in the brain from *TAp73* KO mice suggest that other ciliogenic factors may rescue brain

◀ **Fig. 4** *TAp73* is dispensable for brain multiciliogenesis. **a** The expression of KI-67, Aquaporin 1 (AQP1, green), and ADP-ribosylation factor-like 13b (ARL13B, red) in WT hindbrain roof plate/CP at E14.5. Notice that KI-67⁺ roof plate progenitors, and AQP1⁺ CP epithelial cells are spatially separated. ARL13B labels monociliated roof plate progenitors and multiciliated CP epithelial cells. White lines demarcate roof plate epithelium (KI-67⁺/AQP1⁻, arrows), CP epithelium (KI-67⁻/AQP1⁺, asterisks), and “transition zone” (KI-67⁻/AQP1⁻, arrowheads) in which MCCs appear. Dotted lines mark apical cell surface with cilia. DAPI staining (blue) labels nuclei. **b** Expression of *TAp73* (green, red), AQP1 (green), and ARL13B (red) in WT hindbrain roof plate/CP at E14.5. Dotted lines mark apical cell surface of roof plate (*TAp73*⁻, arrow) and transition zone (*TAp73*⁺, arrowhead). White lines mark transition zone (*TAp73*⁺/AQP1⁻, arrowhead) and CP epithelium (*TAp73*⁺/AQP1⁺, asterisk). DAPI staining (blue) labels nuclei. **c** Representative images of *TAp73* expression of ependymal and CP epithelial cells in hindbrain and lateral ventricle from WT and *TAp73* KO. Red dotted lines mark ventricles lined with ependymal cells. Note that p73 expression is lost in *TAp73* KO mice. **d** Expression of the cilia marker ARL13B (red) in CP epithelial cells from WT and *TAp73* KO. White arrowheads mark cilia on cell surface. DAPI staining (blue) labels nuclei. Quantitation of average cilia length is shown in the lower panel. Data from a single experiment are shown (WT, *n* = 12 cells [hindbrain] and 9 cells [lateral ventricle] from 2 mice; *TAp73* KO, *n* = 17 cells [hindbrain] and 15 cells [lateral ventricle] from 3 mice). **e** Immunoblot analysis of Ac- α -TUB in brain ventricles from WT and *TAp73* KO animals. β -Actin serves as a loading control. Data are representative of two independent experiments. **f** Semiquantitative PCR of *Dnal1*, *Foxj1*, *Rfx2*, and *Rfx3* in brain ventricles from WT and *TAp73* KO. Data from a single experiment are shown (WT, *n* = 3; *TAp73* KO, *n* = 4). **g** Movement of fluorescent beads along the ventricular system in WT and *TAp73* KO mice. Images of maximum intensity projections of representative movies of the lateral and the ventral third ventricles are shown (WT, *n* = 2; *TAp73* KO, *n* = 3; *TAp73* heterozygous, *n* = 1). Red arrows mark the direction of bead flow. Bracket lines depict ependymal layer lining the lateral ventricles. Refer to Supplementary Video S3a, b for examples of recording of ciliary beating. All data are presented as mean \pm SEM and relative to the WT group with **P* < 0.05, ***P* < 0.01

multiciliogenesis in the absence of *TAp73*. *TAp73* influences post-transcriptional mechanisms via regulation of miRNAs [12]. Analysis of small RNA species from brain ventricles in *TAp73* KO mice revealed reduced *miR34bc* levels, along with a strong induction of the *miR449a* and *miR449c* that work together with the *miR-34* cluster to regulate multiciliogenesis in different tissues across species (Fig. 5a, c; Supplementary Table 6) [11, 33, 51–53]. In the brain, *miR449a* is predominantly detected in the CP [54, 55], where its expression undergoes greater than ten-fold increase upon *TAp73* loss, whereas *miR34bc* levels strongly decline (Fig. 5b, c). Although *miR34b* levels were downregulated also in the trachea from *TAp73* KO (Supplementary Fig. 7a), *miR449a* induction was less pronounced and more variable in FTs and EDs (Fig. 5d). Altogether, these results reveal a conserved reaction from the *miR-34/449* family following *TAp73* loss in diverse multiciliated epithelia.

In an effort to understand *miR449* upregulation, we analyzed potential changes in the RB-E2F pathway known to regulate *miR449* levels [56, 57]. However, expression of *E2f1*, *E2f3*, *Cdkn1a*, and *Cdkn1b* in brain ventricles were comparable between WT and mutant animals (Supplementary Fig. 8a, b), indicative of a RB-E2F pathway unaffected by *TAp73* loss in brain MCCs. Interestingly, transcript and protein levels of the other E2F family member E2F4, which is a potent inducer of multiciliogenesis [6–8, 48, 58, 59], were markedly increased in *TAp73* KO ventricles, despite only a mild increase of its cofactor *Mcidas* (Fig. 5e, f). In contrast, E2F4 levels in FTs and EDs were unaltered and even downregulated in tracheae (Supplementary Fig. 7b–e). Therefore, increased E2F4 levels concurrent with a *miR449* increase are restricted to the brain in *TAp73* KO mice.

To assess potential E2F4 contribution to *miR449* elevation, we used the genomic region of *miR449* containing three putative E2F-binding sites in a reporter-based assay. Indeed, E2F4 in combination with MCIDAS elicited a strong transcriptional response from the *miR449* locus, a reaction almost abolished by mutating the strongest out of three E2F consensus motifs (Fig. 5g; Supplementary Table 5). Together, these results indicate that increased E2F4/MCIDAS activity may stimulate *miR449* expression in *TAp73* KO brains.

***TAp73* collaborates with *miR449* in brain multiciliogenesis**

Our data suggest that *miR449* upregulation may compensate at least partially for *TAp73* loss to maintain brain multiciliogenesis. To address this, we generated mice with a deletion of the *miR449* cluster in addition to *TAp73*. Strikingly, *TAp73*^{-/-};*miR449*^{-/-} (*TAp73xmiR449* KO) mice developed severe hydrocephalus, a defect not present in *TAp73* KO or *miR449* KO mice (Fig. 6a; Supplementary Fig. 9a). Since defective ependymal and CP cilia contribute to the development of hydrocephalus [60–62], we next assessed ciliation in the ventricles of *TAp73xmiR449* KO mice. Analysis of the expression of ARL13B in CP epithelium revealed a decrease in cilia number and length in the absence of *miR449*, whereas a more pronounced reduction in cilia was observed in *TAp73xmiR449* KO mice (Fig. 6b, c; Supplementary Fig. 9b). TEM studies also revealed mildly disorganized apical docking of basal bodies in ependymal cells in *TAp73* KO and *TAp73xmiR449* KO mice (Fig. 6d; Supplementary Fig. 9c); however, Ac- α -TUB content was similar in ependymal cells among WT and *TAp73xmiR449* KO animals (Supplementary Fig. 9d). Consistently, ciliary beating and bead flow over ventricles appeared unaffected in *TAp73xmiR449* KO animals (Supplementary Fig. 9e; Supplementary Video 3a, c). Furthermore, expression of cytokeratins, AQP1, and OTX2 in CP

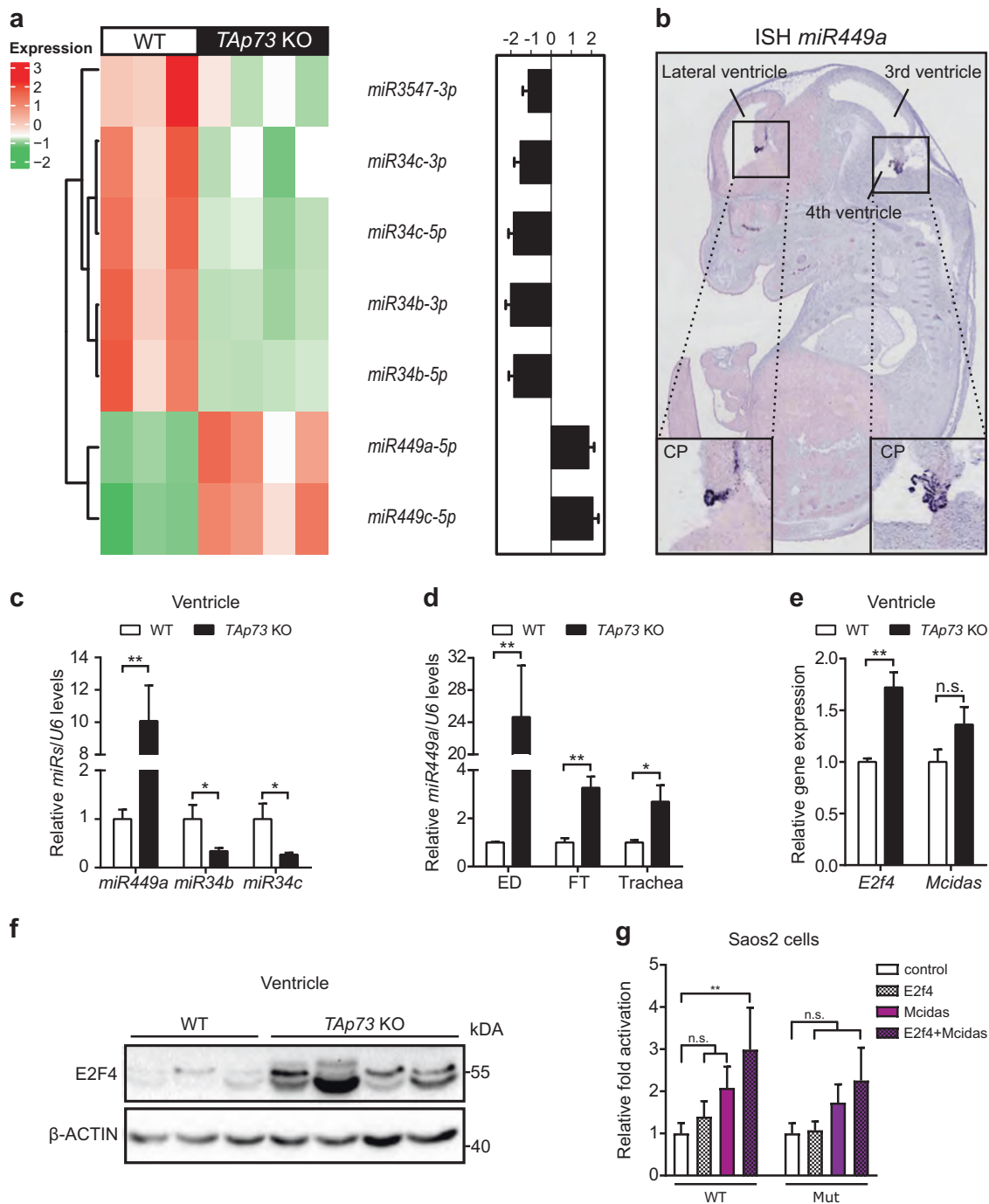
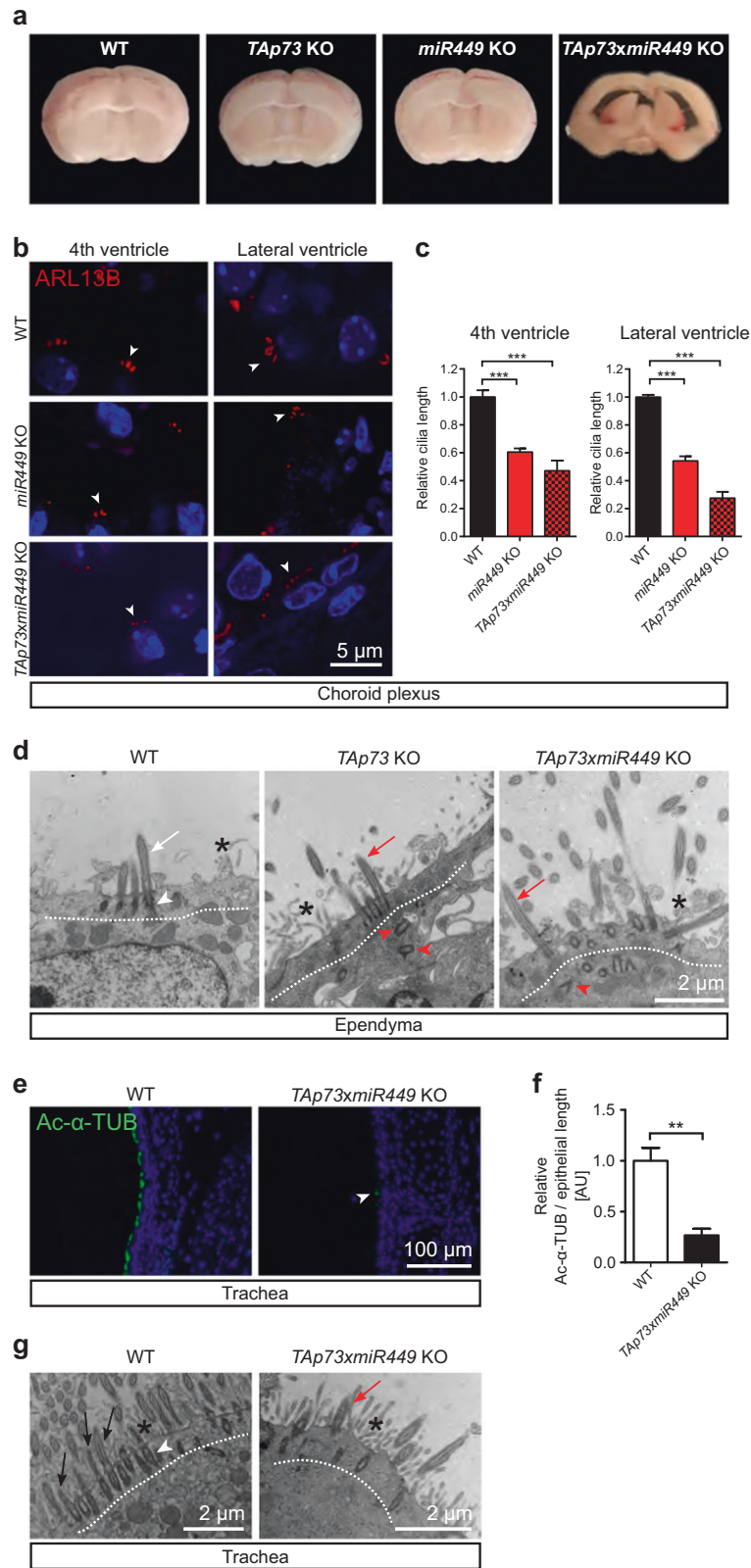


Fig. 5 *TAp73* loss leads to changes in *miR-34/449* family and E2F4/MCIDAS circuit in the brain. **a** Hierarchical clustering of differentially expressed miRNAs in brain ventricles from WT and *TAp73* KO mice (WT, $n = 3$; *TAp73* KO, $n = 4$, one-way ANOVA, FDR < 0.05, fold change is shown). \log_2 values for miRNAs are plotted on the right. **b** In situ hybridization analysis of the expression of *miR449* in WT roof plate/CP at E14.5 (<http://www.eurexpress.org/ee/>) [79]. Semi-quantitative PCR analysis of *miR449a*, *miR34b*, and *miR34c* in brain ventricles (**c**), *miR449a* expression in EDs, FTs, and trachea (**d**), and *E2f4* and *Mcidas* levels in brain ventricles (**e**) from WT and *TAp73* KO mice. Data from a single experiment are shown (WT: ED, $n = 3$; FT, $n = 7$; trachea, $n = 4$; ventricle, $n = 3$. *TAp73* KO: ED, $n = 4$; FT, $n = 8$; trachea, $n = 4$; ventricle, $n = 4$). **f** Immunoblot of E2F4 in

WT and *TAp73* KO ventricles. β -Actin serves as a loading control. Representative result of three independent experiments. **g** The luciferase assay of *miR449* regulatory regions containing E2F-binding motifs. Three consensus E2F-binding sites in *miR449* locus (<http://jaspar.binf.ku.dk/>) were placed in front of a luciferase cassette. A deletion mutant (Mut) that lacks the strongest consensus site was also created (Supplementary Table 5). WT or Mut luciferase vector was then co-transfected with empty vector (control), or vectors expressing E2F4, MCIDAS, or both. Fold changes in luciferase activities relative to those of control vector are shown. Data from five independent experiments are shown. All data are presented as mean \pm SEM and relative to the WT group with * $P < 0.05$, ** $P < 0.01$



epithelial cells was similar among WT, *miR449* KO, and *TAp73xmiR449* KO animals (Supplementary Fig. 10a–c). Despite the role of Notch signaling in CP development and

tumorigenesis [31, 63], RNAscope studies revealed similar expression of Notch targets *Hes1* and *Hes5*, multiciliogenesis regulators *Mcidas* and *Foxj1* in the roof plate

◀ **Fig. 6** TAp73 functions through *miR449* in brain multiciliogenesis. **a** Coronal brain slices from WT, *TAp73* KO, *miR449* KO, and *TAp73xmiR449* KO mice. Note that *TAp73xmiR449* KO mice display enlarged lateral ventricles. **b** ARL13B (red) expression in CP epithelial cells of the fourth and lateral ventricles from WT, *miR449* KO, and *TAp73xmiR449* KO animals. White arrowheads mark cilia on cell surface. DAPI staining (blue) labels nuclei. **c** Quantitation of average cilia length of CP epithelial cells shown in **(b)**. Data from a single experiment are shown (WT, $n = 4$ cells [hindbrain, lateral ventricle] from 2 mice; *miR449* KO, $n = 18$ cells [hindbrain] and 14 cells [lateral ventricle] from 4 mice; *TAp73xmiR449* KO, $n = 8$ cells [hindbrain, lateral ventricle] from 3 mice). **d** Representative TEM photomicrographs of ependymal cells in WT, *TAp73* KO, and *TAp73xmiR449* KO mice. Dotted lines mark apical region of the cells. Notice that WT cells possess cilia (white arrow) and basal bodies (white arrowhead) docked to the apical surface, whereas mutant cells have a similar number of cilia (red arrows) but disorganized basal bodies (red arrowheads) located further away from the apical surface. Interspersed microvilli are marked with asterisks. **e** Representative staining of Ac- α -TUB (green) in tracheae from WT and *TAp73xmiR449* KO mice. DAPI staining (blue) labels nuclei. Note that mutants harbor less and shorter cilia (arrowhead) than WTs. **f** Quantitation of Ac- α -TUB signals normalized to epithelial length is shown. Data from a single experiment are shown ($n = 4$ samples/genotype). **g** Representative TEM photomicrographs of tracheae from WT and *TAp73xmiR449* KO mice. Dotted lines mark apical region of the cells. Notice the abundant cilia (black arrows) and clustered basal bodies (white arrowhead) docked to apical surface in WT cells, whereas mutant cells exhibit fewer cilia (red arrow). Interspersed microvilli are marked with asterisks. All data are presented as mean \pm SEM and relative to the WT group with $**P < 0.01$, $***P < 0.001$

of WT, *miR449* KO, and *TAp73xmiR449* KO embryos at E14.5 (Supplementary Fig. 11). In summary, additional loss of *miR449* in *TAp73* KO mice strongly impairs ciliogenesis in the CP, and slightly affects ependymal cilia, which is consistent with its prominent expression in the CP [54] (Fig. 5b). Thus, our data indicate that *miR449* collaborates with *TAp73* to drive multiciliogenesis in the brain.

As *miR449* was induced upon *TAp73* deletion in further multiciliated tissues, we analyzed tracheae and EDs in *TAp73xmiR449* KO mice. Immunostainings and TEM consistently revealed a dramatic decrease in cilia coverage and an increase in defective basal body docking in trachea from *TAp73xmiR449* KO animals compared to WT animals (Fig. 6e–g; Supplementary Fig. 12a), a phenotype bearing resemblance to our previous findings in the airways of *TAp73* KO animals [12]. Likewise, loss of *miR449* did not further enhance MCC reduction in *TAp73*-deficient EDs (Supplementary Fig. 12b, c). Thus, additional deletion of the *miR449* cluster fails to exacerbate ciliary defects in trachea and EDs in the absence of *TAp73*.

Overall, our data indicate that TAp73 utilizes the unique topology of its transcriptional circuit to communicate with the *miR-34/449* family and other crucial regulators of multiciliogenesis e.g., *E2F4/MCIDAS* to regulate brain multiciliogenesis (Fig. 7a, d, e).

Discussion

TAp73 activates a plethora of ciliogenic effectors to drive multiciliogenesis in the airways [12, 13]. The current study examines the role of TAp73-driven molecular circuit in MCCs of reproductive tracts and the brain. Our results revealed a profound reduction of cilia in EDs and FTs from *TAp73*-deficient mice, as well as diminished *Foxj1*, *Rfx2*, and *Rfx3* expression. These molecular and cellular changes in MCCs are reminiscent of our previous findings in respiratory epithelia of these mice, suggesting that male and female infertility associated with *TAp73* loss could be in part related to the observed cilia loss. The expression of the axonemal dyneins *Dnai1* and *Dnali1*, both of which exhibit TAp73 binding in their genomic loci, was also significantly reduced in EDs and FTs from mutant animals, indicating that they are part of the TAp73-directed multiciliogenesis program in reproductive tracts.

Consistent with previous reports, we found partial degradation of the germinal epithelium and reduced sperm cell production in *TAp73* KO mice [42, 43]. The EDs are comprised of MCCs, which are required for fluid circulation and reabsorption, thereby, facilitating the transport of spermatozoa to their storage and maturation in the Epi [22, 24, 25]. Despite the presence of flagellated spermatozoa in testis, lack of spermatozoa in Epi of *TAp73* KO mice indicates that defective multiciliogenesis may contribute to male sterility. Indeed, disruption of transcriptional and post-transcriptional regulators of multiciliogenesis has been shown to cause infertility in mice and humans [3, 64, 65], whereas fertility issues have been reported in female primary ciliary dyskinesia patients [20, 21]. Importantly, *TAp73* is downregulated as women age [66], and certain single nucleotide polymorphisms in *TP73* are associated with female patients over 35 years of age seeking in vitro fertilization [67, 68]. Hence, the integrity of MCCs is critical for reproductive health. Further studies using tissue-specific deletion of *TAp73* in MCCs of EDs and oviducts are necessary to delineate its role in reproductive motile cilia maintenance and fertility.

In the brain, *TAp73* expression is initiated at the onset of multiciliated differentiation of ependymal and CP epithelial cells. However, our data indicate that *TAp73* is dispensable for the generation of cilia in the brain, although it is plausible that *TAp73* loss results in more subtle defects such as polarity and cilia orientation [69, 70]. In contrast to the dynamic TAp73-dependent program in the airways and reproductive tracts, expression of *Foxj1*, *Rfx2*, and *Rfx3* in the brain remains mostly unaltered in the absence of *TAp73*, suggesting that other effectors maintain the activity of the molecular circuit to support MCC differentiation.

Previous studies revealed robust expression of *GemC1* and *E2f/Mcidas*, all of which are capable of transcriptional

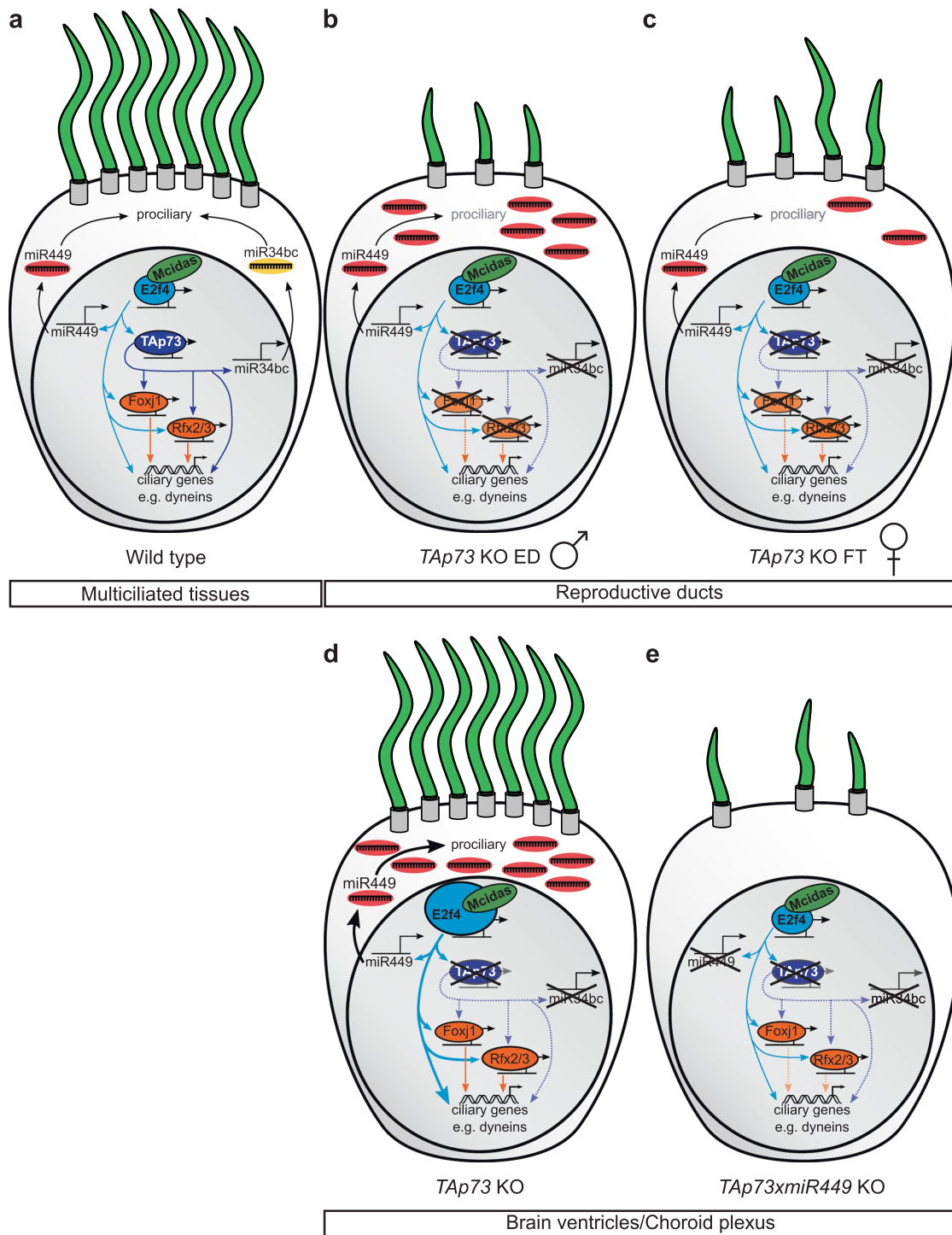


Fig. 7 Schematic diagram of the molecular circuits of TAp73-driven multiciliogenesis in diverse tissues. **a** TAp73-dependent transcriptional network, including dyneins, *miR34bc*, *Foxj1*, *Rfx2*, and *Rfx3* factors, critically regulates multiciliogenesis in various ciliated epithelia downstream of *E2f4/Mcidas*. In the EDs (**b**) and FTs (**c**) *TAp73* KO impairs multiciliogenesis concurrent with male and female infertility.

d *TAp73* is not essential for multiciliogenesis in the brain; however, *TAp73* loss leads to upregulation of pro-ciliogenic *E2f4* and its target *miR449*. **e** Further removal of *miR449* in *TAp73* KO animals leads to reduced number and length of CP cilia and severe hydrocephalus, indicating that *miR449* and TAp73 complement each other to support brain ciliogenesis

activation of *Foxj1*, *TAp73* itself, and many other ciliogenic effectors e.g., *Rfx2* and *Rfx3*, in MCCs of the brain [4, 6, 8, 48, 71]. Indeed, E2F4/MCIDAS expression is

upregulated in the brain but not in other multiciliated tissues upon *TAp73* loss, and therefore may facilitate brain multiciliogenesis. In agreement, loss of either *Mcidas* or *GemC1*,

both transcriptional activators of *TAp73*, leads to defect in MCC differentiation and hydrocephalus [3, 6].

Although it is less clear how *TAp73* loss results in enhanced E2F/MCIDAS activity in the brain, a quick look downstream of *TAp73* provides some clues: reduced expression of the *TAp73* target *miR34bc* is concurrent with an induction of *miR449* in the absence of *TAp73*. Interestingly, expression of *Cdkn1alp21*, *Cdkn1blp27*, *E2f1*, and *E2f3* in brain ventricles remain unchanged following *TAp73* loss, suggesting that *TAp73* loss regulates E2F and *miR449* activity independently of the conserved RB-E2F1 axis. *miR449* induction is commonly observed in *miR-34*-deficient MCCs, whereas ablation of the entire *miR-34/449* family severely impairs multiciliogenesis in diverse tissues [33, 65, 72]. The redundancy might explain why a loss of the *miR449* cluster failed to worsen ciliary defects outside the brain in *TAp73* KO animals. In contrast, *miR449* cluster is prominently expressed in MCCs in the brain, where its loss alone is sufficient to impact multiciliogenesis, indicating a unique role for *miR449* in brain MCCs. *miR449* is known to inhibit the Notch pathway to relieve the suppression of MCC fate determination; however, Notch pathway activity as well as the expression of *Mcidas* and *Foxj1* in the roof plate and the CP remains unchanged after *miR449* loss. Thus, it is plausible that *miR449* may indirectly increase E2F/MCIDAS activity in MCCs of the brain independent of Notch inhibition and *Mcidas* derepression. Conversely, transcriptional activation of *miR449* by E2F/MCIDAS complexes may complete the feedback loop to keep the molecular circuit fully engaged in the absence of *TAp73*.

This interpretation posits that the crosstalk between *miR449* and E2F/MCIDAS serves as a crucial backup circuit for *TAp73*-driven multiciliogenesis network in the brain. Indeed, combined deletion of *TAp73* and *miR449* results in disruption of multiciliogenesis in the brain and hydrocephalus, defects distinct from those associated with loss of either *TAp73* or *miR449* alone, or complete loss of the *miR-34/449* family [33, 73]. Strikingly, in *TAp73*-deficient MCCs outside the brain that exhibit less prominent increase in *miR449* and no increase in E2F4 levels, further deletion of *miR449* cluster fails to exacerbate multiciliogenesis defects caused by *TAp73* loss, indicating that *TAp73* functions at least partially through *miR449* to support MCCs in the brain. Recent studies also demonstrated the role of *TAp73*-driven *miR34a* expression in neuronal development [74]. Therefore, interaction of *TAp73* with *miR-34/449* family members is crucial for normal brain functions.

Nonetheless, detailed studies are necessary to clarify the interaction between *miR449* and E2F4/MCIDAS pathway in MCCs in the brain, but also to address *miR449* regulation in *TAp73*-deficient MCCs outside the brain.

Unlike *TAp73* mutant animals, *p73* KO mice lacking both *TAp73* and $\Delta Np73$ exhibit hydrocephalus, defective

ependymal cell maturation and aqueduct stenosis, suggesting a potential role for $\Delta Np73$ in ependymal cells [75, 76]. Given the abnormal apical localization of basal bodies in ependymal cells along with ciliary defects in the CP from *TAp73xmiR449* KO mice, it is conceivable that $\Delta Np73$ may regulate *miR449* expression indirectly in these cells. In support of this notion, *miR449* is highly expressed in the CP whereby its loss alone leads to ciliary defects, whereas $\Delta Np73$ deletion also results in defects in the CP [77]. Further analysis of the multiciliogenesis network and *miR449* expression in MCCs in the brains of *p73* KO and $\Delta Np73$ KO animals are necessary to resolve these questions.

Acknowledgements We thank Tak Mak for providing *TAp73* KO mice, Gerd Hasenfuß for support, Matthias Döbelstein for hosting, and Karola Metze and Verena Siol for assistance. ML is supported by the Deutsche Forschungsgemeinschaft (DFG Li 2405); HZ by the New York Institute of Technology, Sanford Research, Matthew Larson Foundation, Institutional Development Award from the National Institute of General Medical Sciences under grant numbers 5P20GM103548, 1P20GM103620-01A1, and the National Cancer Institute (R01CA220551); FB by Wilhelm-Sander-Stiftung (2016.041.1); AKG by the Max Planck Society. We thank Heymut Omran's group for introduction to cilia microscopy and Travis Stracker for disclosure of unpublished data.

Author contributions MeW and TE characterized cilia defects and gene expression and generated figures. MeW and MaW validated *TAp73* targets by WB and ChIP. EE and FB contributed IF analysis of human epididymis. EE performed cilia quantification on tracheae. DR performed electron microscopy analysis. CW and SB maintained mice. CW performed RNA isolations and qPCRs. LV-H and SB contributed to western blot analysis of different tissues. ZH performed RNAscope analysis for *TAp73* on diverse tissues. KBG, JZ, LL, and HZ contributed brain analyses. A-KG analyzed ex vivo ciliary beating. OS analyzed small RNA sequencing data. SA contributed to interpretation and supported the group. ML developed the project, interpreted the data, designed and coordinated the experiments to complete this study. MeW, TE, HZ, and ML were major contributors to manuscript preparation.

Compliance with ethical standards

Conflict of interest The authors declare that they have no conflict of interest.

Publisher's note: Springer Nature remains neutral with regard to jurisdictional claims in published maps and institutional affiliations.

References

- Spassky N, Meunier A. The development and functions of multiciliated epithelia. *Nat Rev Mol Cell Biol.* 2017;18:423–36.
- Choksi SP, Lauter G, Swoboda P, Roy S. Switching on cilia: transcriptional networks regulating ciliogenesis. *Development.* 2014;141:1427–41.
- Terré B, Piergiovanni G, Segura-Bayona S, Gil-Gómez G, Youssef SA, Attolini CS-O, et al. GEMC1 is a critical regulator of multiciliated cell differentiation. *EMBO J.* 2016;35:942–60.
- Arbi M, Pefani D-E, Kyrousi C, Lalioti M-E, Kalogeropoulou A, Papanastasiou AD, et al. GemC1 controls multiciliogenesis in the airway epithelium. *EMBO Rep.* 2016;17:400–13.

5. Zhou F, Narasimhan V, Shboul M, Chong YL, Reversade B, Roy S. Gmnc is a master regulator of the multiciliated cell differentiation program. *Curr Biol*. 2015;25:3267–73.
6. Boon M, Wallmeier J, Ma L, Loges NT, Jaspers M, Olbrich H, et al. MCIDAS mutations result in a mucociliary clearance disorder with reduced generation of multiple motile cilia. *Nat Commun*. 2014;5:4418.
7. Ma L, Quigley I, Omran H, Kintner C. Multicilin drives centriole biogenesis via E2f proteins. *Genes Dev*. 2014;28:1461–71.
8. Stubbs JL, Vladar EK, Axelrod JD, Kintner C. Multicilin promotes centriole assembly and ciliogenesis during multiciliate cell differentiation. *Nat Cell Biol*. 2012;14:140–7.
9. Danielian PS, Hess RA, Lees JA. E2f4 and E2f5 are essential for the development of the male reproductive system. *Cell Cycle*. 2016;15:250–60.
10. Danielian PS, Bender Kim CF, Caron AM, Vasile E, Bronson RT, Lees JA. E2f4 is required for normal development of the airway epithelium. *Dev Biol*. 2007;305:564–76.
11. Marcet B, Chevalier B, Luxardi G, Coraux C, Zaragosi L-E, Cibois M, et al. Control of vertebrate multiciliogenesis by miR-449 through direct repression of the Delta/Notch pathway. *Nat Cell Biol*. 2011;13:693–9.
12. Nemajerova A, Kramer D, Siller SS, Herr C, Shomroni O, Pena T, et al. TAp73 is a central transcriptional regulator of airway multiciliogenesis. *Genes Dev*. 2016;30:1300–12.
13. Marshall CB, Mays DJ, Beeler JS, Rosenbluth JM, Boyd KL, Santos Guasch GL, et al. p73 is required for multiciliogenesis and regulates the Foxj1-associated gene network. *Cell Rep*. 2016;14:2289–300.
14. Blatt EN, Yan XH, Wuerffel MK, Hamilos DL, Brody SL. Forkhead transcription factor HFH-4 expression is temporally related to ciliogenesis. *Am J Respir Cell Mol Biol*. 1999;21:168–76.
15. Brody SL, Yan XH, Wuerffel MK, Song SK, Shapiro SD. Ciliogenesis and left-right axis defects in forkhead factor HFH-4 null mice. *Am J Respir Cell Mol Biol*. 2000;23:45–51.
16. Chen J, Knowles HJ, Hebert JL, Hackett BP. Mutation of the mouse hepatocyte nuclear factor/forkhead homologue 4 gene results in an absence of cilia and random left-right asymmetry. *J Clin Invest*. 1998;102:1077–82.
17. Yu X, Ng CP, Habacher H, Roy S. Foxj1 transcription factors are master regulators of the motile ciliogenic program. *Nat Genet*. 2008;40:1445–53.
18. Crow J, Amso NN, Lewin J, Shaw RW. Morphology and ultrastructure of fallopian tube epithelium at different stages of the menstrual cycle and menopause. *Hum Reprod*. 1994;9:2224–33.
19. Lyons RA, Saridogan E, Djahanbakhch O. The reproductive significance of human Fallopian tube cilia. *Hum Reprod Update*. 2006;12:363–72.
20. Raidt J, Werner C, Menchen T, Dougherty GW, Olbrich H, Loges NT, et al. Ciliary function and motor protein composition of human fallopian tubes. *Hum Reprod*. 2015;30:2871–80.
21. Vanaken GJ, Bassinet L, Boon M, Mani R, Honoré I, Papon J-F, et al. Infertility in an adult cohort with primary ciliary dyskinesia: phenotype–gene association. *Eur Respir J*. 2017;50:1700314.
22. Ilio KY, Hess RA. Structure and function of the ductuli efferentes: a review. *Microsc Res Tech*. 1994;29:432–67.
23. Lambert M-AH, Mendive F, Laurent P, Van Schoore G, Noël J-C, Vanderhaeghen P, et al. Three-dimensional reconstruction of efferent ducts in wild-type and Lgr4 knock-out mice. *Anat Rec*. 2009;292:595–603.
24. Hess RA. The efferent ductules: structure and functions [Internet]. In: Robaire B, Hinton BT, editors. *The epididymis: from molecules to clinical practice*. Boston, MA: Springer US; 2002. [cited 2017 Jan 19]. p. 49–80. Available from: http://link.springer.com/10.1007/978-1-4615-0679-9_4.
25. Hess RA. Small tubules, surprising discoveries: from efferent ductules in the turkey to the discovery that estrogen receptor alpha is essential for fertility in the male. *Anim Reprod*. 2015;12:7–23.
26. Lun MP, Johnson MB, Broadbelt KG, Watanabe M, Kang Y-J, Chau KF, et al. Spatially heterogeneous choroid plexus transcriptomes encode positional identity and contribute to regional CSF production. *J Neurosci*. 2015;35:4903–16.
27. Silva-Vargas V, Maldonado-Soto A, Mizrak D, Codega P, Doetsch F. Age-dependent niche signals from the choroid plexus regulate adult neural stem cells. *Cell Stem Cell*. 2016;19:643–52.
28. Spassky N, Merkle FT, Flames N, Tramontin AD, García-Verdugo JM, Alvarez-Buylla A. Adult ependymal cells are post-mitotic and are derived from radial glial cells during embryogenesis. *J Neurosci J Soc Neurosci*. 2005;25:10–8.
29. Lun MP, Monuki ES, Lehtinen MK. Development and functions of the choroid plexus-cerebrospinal fluid system. *Nat Rev Neurosci*. 2015;16:445–57.
30. Del Bigio MR. Ependymal cells: biology and pathology. *Acta Neuropathol*. 2010;119:55–73.
31. Li L, Gausam KB, Wang J, Lun MP, Ohli J, Lidov HGW, et al. Sonic hedgehog promotes proliferation of Notch-dependent monociliated choroid plexus tumour cells. *Nat Cell Biol*. 2016;18:418–30.
32. Tomasini R, Tsuchihara K, Wilhelm M, Fujitani M, Rufini A, Cheung CC, et al. TAp73 knockout shows genomic instability with infertility and tumor suppressor functions. *Genes Dev*. 2008;22:2677–91.
33. Song R, Walentek P, Sponer N, Klimke A, Lee JS, Dixon G, et al. miR-34/449 miRNAs are required for motile ciliogenesis by repressing cp110. *Nature*. 2014;510:115–20.
34. Schindelin J, Arganda-Carreras I, Frise E, Kaynig V, Longair M, Pietzsch T, et al. Fiji: an open-source platform for biological-image analysis. *Nat Methods*. 2012;9:676–82.
35. Capece V, Garcia Vizcaino JC, Vidal R, Rahman R-U, Pena Centeno T, Shomroni O, et al. Oasis: online analysis of small RNA deep sequencing data. *Bioinformatics*. 2015;31:2205–7.
36. Martin M. Cutadapt removes adapter sequences from high-throughput sequencing reads. *EMBnet J*. 2011;17:10.
37. Dobin A, Davis CA, Schlesinger F, Drenkow J, Zaleski C, Jha S, et al. STAR: ultrafast universal RNA-seq aligner. *Bioinformatics*. 2013;29:15–21.
38. Liao Y, Smyth GK, Shi W. featureCounts: an efficient general purpose program for assigning sequence reads to genomic features. *Bioinformatics*. 2014;30:923–30.
39. Friedländer MR, Mackowiak SD, Li N, Chen W, Rajewsky N. miRDeep2 accurately identifies known and hundreds of novel microRNA genes in seven animal clades. *Nucleic Acids Res*. 2012;40:37–52.
40. Love MI, Huber W, Anders S. Moderated estimation of fold change and dispersion for RNA-seq data with DESeq2. *Genome Biol*. 2014;15:550.
41. Faubel R, Westendorf C, Bodenschatz E, Eichele G. Cilia-based flow network in the brain ventricles. *Science*. 2016;353:176–8.
42. Holembowski L, Kramer D, Riedel D, Sordella R, Nemajerova A, Dobbstein M, et al. TAp73 is essential for germ cell adhesion and maturation in testis. *J Cell Biol*. 2014;204:1173–90.
43. Inoue S, Tomasini R, Rufini A, Elia AJ, Agostini M, Amelio I, et al. TAp73 is required for spermatogenesis and the maintenance of male fertility. *Proc Natl Acad Sci USA*. 2014;111:1843–8.
44. Dacheux J-L, Dacheux F. New insights into epididymal function in relation to sperm maturation. *Reproduction*. 2013;147:R27–42.
45. Mendive F, Laurent P, Van Schoore G, Skarnes W, Pochet R, Vassart G. Defective postnatal development of the male reproductive tract in LGR4 knockout mice. *Dev Biol*. 2006;290:421–34.

46. Santos Guasch GL, Beeler JS, Marshall CB, Shaver TM, Sheng Q, Johnson KN, et al. p73 is required for ovarian follicle development and regulates a gene network involved in cell-to-cell adhesion. *iScience*. 2018;8:236–49.
47. Huang X, Ketova T, Fleming JT, Wang H, Dey SK, Litingtung Y, et al. Sonic hedgehog signaling regulates a novel epithelial progenitor domain of the hindbrain choroid plexus. *Development*. 2009;136:2535–43.
48. Kyrrousi C, Lalioti M-E, Skavatsou E, Lygerou Z, Taraviras S. Mcidas and GemC1/Lynkeas specify embryonic radial glial cells. *Neurogenesis*. 2016;3:e1172747.
49. Mori M, Hazan R, Danielian PS, Mahoney JE, Li H, Lu J, et al. Cytoplasmic E2f4 forms organizing centres for initiation of centriole amplification during multiciliogenesis. *Nat Commun*. 2017;8:15857.
50. Caspary T, Larkins CE, Anderson KV. The graded response to sonic hedgehog depends on cilia architecture. *Dev Cell*. 2007;12:767–78.
51. Lizé M, Herr C, Klimke A, Bals R, Dobbstein M. MicroRNA-449a levels increase by several orders of magnitude during mucociliary differentiation of airway epithelia. *Cell Cycle*. 2010;9:4579–83.
52. Marcet B, Chevalier B, Coraux C, Kodjabachian L, Barbry P. MicroRNA-based silencing of Delta/Notch signaling promotes multiple cilia formation. *Cell Cycle*. 2011;10:2858–64.
53. Otto T, Candido SV, Pilarz MS, Sicinska E, Bronson RT, Bowden M, et al. Cell cycle-targeting microRNAs promote differentiation by enforcing cell-cycle exit. *Proc Natl Acad Sci USA*. 2017;114:10660–5.
54. Redshaw N, Wheeler G, Hajihosseini MK, Dalmay T. microRNA-449 is a putative regulator of choroid plexus development and function. *Brain Res*. 2009;1250:20–6.
55. Shu P, Wu C, Liu W, Ruan X, Liu C, Hou L, et al. The spatiotemporal expression pattern of MicroRNA in the developing mouse nervous system. *J Biol Chem*. 2018;294:3444–53. jbc.RA118.004390
56. Yang X, Feng M, Jiang X, Wu Z, Li Z, Aau M, et al. miR-449a and miR-449b are direct transcriptional targets of E2F1 and negatively regulate pRb-E2F1 activity through a feedback loop by targeting CDK6 and CDC25A. *Genes Dev*. 2009;23:2388–93.
57. Lizé M, Pilarski S, Dobbstein M. E2F1-inducible microRNA 449a/b suppresses cell proliferation and promotes apoptosis. *Cell Death Differ*. 2010;17:452–8.
58. Kyrrousi C, Arbi M, Pilz G-A, Pefani D-E, Lalioti M-E, Ninkovic J, et al. Mcidas and GemC1 are key regulators for the generation of multiciliated ependymal cells in the adult neurogenic niche. *Development*. 2015;142:3661–74.
59. Kim S, Ma L, Shokhirev MN, Quigley I, Kintner C. Multicilin and activated E2f4 induce multiciliated cell differentiation in primary fibroblasts. *Sci Rep*. 2018;8:12369.
60. Ibanez-Tallon I. Dysfunction of axonemal dynein heavy chain Mdnah5 inhibits ependymal flow and reveals a novel mechanism for hydrocephalus formation. *Hum Mol Genet*. 2004;13:2133–41.
61. Banizs B, Pike MM, Millican CL, Ferguson WB, Komlosi P, Sheetz J, et al. Dysfunctional cilia lead to altered ependyma and choroid plexus function, and result in the formation of hydrocephalus. *Development*. 2005;132:5329–39.
62. Banizs B, Komlosi P, Bevenssee MO, Schwiebert EM, Bell PD, Yoder BK. Altered pH(i) regulation and Na(+)/HCO3(−) transporter activity in choroid plexus of cilia-defective Tg737(orpk) mutant mouse. *Am J Physiol Cell Physiol*. 2007;292:C1409–1416.
63. Bill BR, Balciunas D, McCarra JA, Young ED, Xiong T, Spahn AM, et al. Development and Notch signaling requirements of the zebrafish choroid plexus. *PLoS ONE* 2008;3:e3114.
64. Amirav I, Wallmeier J, Loges NT, Menchen T, Pennekamp P, Mussaffi H, et al. Systematic analysis of CCNO variants in a defined population: implications for clinical phenotype and differential diagnosis. *Hum Mutat*. 2016;37:396–405.
65. Yuan S, Liu Y, Peng H, Tang C, Hennig GW, Wang Z, et al. Motile cilia of the male reproductive system require miR-34/miR-449 for development and function to generate luminal turbulence. *Proc Natl Acad Sci USA*. 2019;116:201817018.
66. Guglielmino MR, Santonocito M, Vento M, Ragusa M, Barbagallo D, Borzi P, et al. TAp73 is downregulated in oocytes from women of advanced reproductive age. *Cell Cycle*. 2011;10:3253–6.
67. Hu W, Zheng T, Wang J. Regulation of fertility by the p53 family members. *Genes Cancer*. 2011;2:420–30.
68. Feng Z, Zhang C, Kang H-J, Sun Y, Wang H, Naqvi A, et al. Regulation of female reproduction by p53 and its family members. *FASEB J Publ Fed Am Soc Exp Biol*. 2011;25:2245–55.
69. Fujitani M, Sato R, Yamashita T. Loss of p73 in ependymal cells during the perinatal period leads to aqueductal stenosis. *Sci Rep*. 2017;7:12007.
70. Gonzalez-Cano L, Fuertes-Alvarez S, Robledinos-Anton N, Bizy A, Villena-Cortes A, Fariñas I, et al. p73 is required for ependymal cell maturation and neurogenic SVZ cytoarchitecture. *Dev Neurobiol*. 2016;76:730–47.
71. Pefani D-E, Dimaki M, Spella M, Karantzelis N, Mitsiki E, Kyrrousi C, et al. Idas, a novel phylogenetically conserved geminin-related protein, binds to geminin and is required for cell cycle progression. *J Biol Chem*. 2011;286:23234–46.
72. Bao J, Li D, Wang L, Wu J, Hu Y, Wang Z, et al. MicroRNA-449 and MicroRNA-34b/c function redundantly in murine testes by targeting E2F transcription factor-retinoblastoma protein (E2F-pRb) pathway. *J Biol Chem*. 2012;287:21686–98.
73. Fededa JP, Esk C, Mierzwa B, Stanyte R, Yuan S, Zheng H, et al. MicroRNA-34/449 controls mitotic spindle orientation during mammalian cortex development. *EMBO J*. 2016;35:2386–98.
74. Agostini M, Tucci P, Killick R, Candi E, Sayan BS, Rivetti di Val Cervo P, et al. Neuronal differentiation by TAp73 is mediated by microRNA-34a regulation of synaptic protein targets. *Proc Natl Acad Sci USA*. 2011;108:21093–8.
75. Medina-Bolívar C, González-Arnay E, Talos F, González-Gómez M, Moll UM, Meyer G. Cortical hypoplasia and ventriculomegaly of p73-deficient mice: developmental and adult analysis: p73 in developing and adult cortex. *J Comp Neurol*. 2014;522:2663–79.
76. Yang A, Walker N, Bronson R, Kaghad M, Oosterwegel M, Bonnin J, et al. p73-deficient mice have neurological, pheromonal and inflammatory defects but lack spontaneous tumours. *Nature*. 2000;404:99–103.
77. Tissir F, Ravni A, Achouri Y, Riethmacher D, Meyer G, Goffinet AM. DeltaNp73 regulates neuronal survival in vivo. *Proc Natl Acad Sci USA*. 2009;106:16871–6.
78. Koeppl M, van Heeringen SJ, Kramer D, Smeenk L, Janssen-Megens E, Hartmann M, et al. Crosstalk between c-Jun and TAp73alpha/beta contributes to the apoptosis-survival balance. *Nucleic Acids Res*. 2011;39:6069–85.
79. Diez-Roux G, Banfi S, Sultan M, Geffers L, Anand S, Rozado D, et al. A high-resolution anatomical atlas of the transcriptome in the mouse embryo. *PLoS Biol*. 2011;9:e1000582.

Affiliations

Merit Wildung¹ · Tilman Uli Esser¹ · Katie Baker Grausam^{2,3} · Cornelia Wiedwald¹ · Larisa Volceanov-Hahn¹ · Dietmar Riedel⁴ · Sabine Beuermann¹ · Li Li² · Jessica Zylla² · Ann-Kathrin Guenther⁵ · Magdalena Wienken⁶ · Evrim Ercetin¹ · Zhiyuan Han⁷ · Felix Bremmer⁸ · Orr Shomroni⁹ · Stefan Andreas¹ · Haotian Zhao^{2,3,7} · Muriel Lizé¹

¹ Molecular & Experimental Pneumology Group, Clinic for Cardiology and Pneumology, University Medical Center Goettingen, Goettingen, Germany

² Cancer Biology and Immunotherapeutics Group, Sanford Research, Sioux Falls, SD, USA

³ Division of Basic Biomedical Sciences, University of South Dakota, Sanford School of Medicine, Vermillion, SD, USA

⁴ Electron Microscopy, Max-Planck-Institute for Biophysical Chemistry, Goettingen, Germany

⁵ Department of Genes and Behavior, MPI for Biophysical

Chemistry, Goettingen, Germany

⁶ Institute of Molecular Oncology, University Medical Center Goettingen, Goettingen, Germany

⁷ Department of Biomedical Sciences, New York Institute of Technology College of Osteopathic Medicine, Old Westbury, NY, USA

⁸ Institute of Pathology, University Medical Center Goettingen, Goettingen, Germany

⁹ Microarray and Deep-Sequencing Core Facility, University Medical Center Goettingen, Goettingen, Germany